

## Experimental Study of a 28 GHz High-Power Long-Pulse Cyclotron Autoresonance Maser Oscillator

S. Alberti, B. G. Danly, G. Gulotta, E. Giguet,\* T. Kimura, W. L. Menninger,  
J. L. Rullier, and R. J. Temkin

*Plasma Fusion Center, Massachusetts Institute of Technology, Cambridge, Massachusetts 02139*  
(Received 29 January 1993)

Experimental results of the first efficient operation of a long-pulse cyclotron autoresonance maser oscillator are presented. Output power of 1.9 MW for a beam energy of 450 keV and current of 80 A, corresponding to an efficiency of 5.2%, has been measured at 27.8 GHz in the TE<sub>11</sub> mode of a Bragg resonator. The observed frequency of the cyclotron autoresonance maser emission corresponds to a Doppler upshifted frequency of 2.9 times the relativistic cyclotron frequency. A significant mode competition between the TE<sub>11</sub> and a TM<sub>01</sub> mode is present.

PACS numbers: 42.52.+x, 52.75.Ms, 85.10.Jz

In recent years, intensive research has been conducted on novel sources of high-power radiation at microwave and millimeter wavelengths. Important advances have been reported in research on electron cyclotron masers such as the gyrotron [1,2], cyclotron autoresonance masers (CARM) [3-8], Cherenkov sources [9], free electron lasers (FEL) [10-12], and other novel devices. For applications such as electron cyclotron heating (ECRH) of fusion plasmas, where high average power is needed, the CARM represents a potential alternative to the gyrotron as a source of high power in the millimeter wave band.

In both sources, the gyrotron and the CARM, the rf generation is based on the cyclotron maser instability which occurs when a relativistic electron beam undergoing motion in a uniform magnetic field  $B_z \mathbf{e}_z$  interacts with a copropagating electromagnetic wave  $(\omega, \mathbf{k})$ , where  $\omega/2\pi$  and  $\mathbf{k}$  are the wave frequency and wave vector, respectively. The cyclotron resonance condition is  $\omega = n\Omega_{c0}/\gamma + k_z v_z$ , where  $n (=1, 2, 3, \dots)$  is the harmonic number,  $\Omega_{c0} = eB_z/m$  is the nonrelativistic cyclotron frequency, where  $m$  and  $e$  are the electron mass and charge, respectively;  $\gamma = (1 - \beta^2)^{-1/2}$  is the relativistic factor where  $\beta = v/c$  and  $v$  is the beam velocity,  $c$  is the speed of light;  $k_z$  and  $v_z$  are the axial wave number and velocity, respectively. The above resonance condition can be rewritten as

$$\omega = \frac{n\Omega_{c0}/\gamma}{1 - \beta_z/\beta_{ph}}, \quad (1)$$

where  $\beta_z = v_z/c$ , and  $\beta_{ph} = \omega/ck_z$  are the normalized electron parallel velocity and phase velocity, respectively. In a cylindrical waveguide, the TE or TM modes are excited when the beam dispersion relation, Eq. (1), and the waveguide dispersion relation are satisfied, the latter being given by

$$\frac{\omega^2}{c^2} = k_z^2 + k_{\perp}^2, \quad (2)$$

where  $k_{\perp} = v_{mp}/r_1$ ,  $r_1$  is the waveguide radius, and  $v_{mp}$  is the  $p$ th zero of  $J'_m(x)$  for TE modes [or the  $p$ th zero of  $J_m(x)$  for TM modes], and  $J_m(x)$  is the ordinary Bessel function. For the case of a constant amplitude free space

wave, the following relationship holds [13]:

$$\frac{d}{dt} [\gamma(1 - \beta_z\beta_{ph})] = 0. \quad (3)$$

Therefore, in the case of a luminous wave ( $\beta_{ph} = 1$ ), an electron which is injected in resonance with the wave will remain in resonance as can be seen from Eq. (1). This effect is called cyclotron autoresonance. The potential for high-efficiency operation of the CARM results from operation near exact autoresonance ( $\beta_{ph} = 1$ ) [3]. A principal advantage of the CARM over the gyrotron ( $\beta_{ph} \rightarrow \infty$ ) is the large Doppler upshift of the operating frequency from the relativistic cyclotron frequency; thus, very high-frequency microwaves can be obtained from the CARM for a relativistic electron beam ( $\beta_z \approx 1$ ) in moderate magnetic fields. Recent CARM oscillator and amplifier experiments have been reported both in the United States [6,8,14] and in Russia [7,15]. All these previous experiments were performed in the short-pulse regime (typically  $\leq 100$  ns) by using a field emission cathode, which intrinsically limits the pulse length, in this regime, power up to 30 MW with a corresponding efficiency of 10% have been obtained [7]. Operation of high-power microwave devices at short-pulse lengths,  $\sim 100$  ns, can eliminate mode competition from parasitic modes, which may have insufficient time to grow to saturation. Modes with high quality factor  $Q$  also cannot be observed in short-pulse operation. The present results in 0.5-1  $\mu$ s operation are long enough for a multimode time equilibrium to be established.

In this Letter we present experimental results of a 27.8 GHz CARM oscillator operated in the long-pulse regime (1  $\mu$ s) at power levels of 1.9 MW with a Pierce-type thermionic electron gun. The normalized phase velocity for the observed TE<sub>11</sub> cylindrical-waveguide mode is  $\beta_{ph} = 1.087$  which confirms operation in the autoresonance regime.

A schematic of the CARM oscillator experiment is shown in Fig. 1. The main components of the device are the high-voltage pulse-forming-network (PFN) type modulator, the thermionic Pierce-type electron gun, the axial guiding magnetic field coils, the bifilar wiggler, and the Bragg resonator.

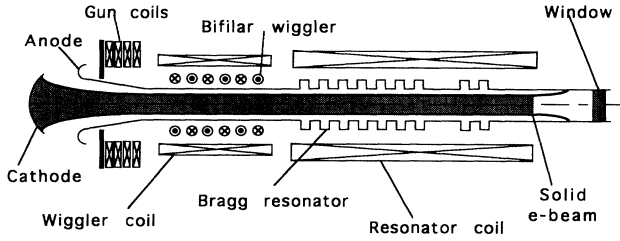


FIG. 1. Schematic of the experimental setup.

The high-voltage  $2.5 \mu\text{s}$  ( $1 \mu\text{s}$  flattop) pulse modulator provides the accelerating potential (450 kV) to the electron gun which has a measured perveance of  $0.27 \mu\text{P}$  ( $P=1 \text{ A/V}^{3/2}$ ). A near periodic transverse magnetic (wiggler) field is used to impart transverse momentum to the electron beam. At the entrance of the bifilar wiggler the axial magnetic guide field has a value of  $B_{wz}=1.92 \text{ kG}$  and the beam radius and normalized emittance, calculated from a gun trajectory code, are  $r_b=4 \text{ mm}$  and  $\epsilon_n=110 \text{ mm mrad}$ , respectively.

As the electron beam enters the bifilar wiggler it resonantly interacts with a helical transverse magnetic field which converts parallel momentum to perpendicular momentum, with the resonant condition given by  $\Omega_{cw} = c\gamma\beta_z k_w$  where  $\Omega_{cw} = eB_{wz}/m$  is the electron cyclotron frequency in the axial wiggler field,  $B_{wz}$ , and  $k_w = 2\pi/\lambda_w$  with  $\lambda_w$  being the wiggler period. In the approximation of the small transverse wiggler field, ( $B_{\perp w} \ll B_{wz}$ ), at resonance the normalized perpendicular velocity  $\beta_{\perp}$  varies linearly with the axial distance and is given by [16]  $\beta_{\perp}(z) = (a_w/\gamma)k_w z$ , where  $a_w = eB_{\perp w}/mck_w$  and  $z$  is the distance from the entrance of the wiggler. In this experiment, the wiggler has  $N_w=4$  periods with a wiggler period of  $\lambda_w=8.57 \text{ cm}$ . For a wiggler current of  $I_w=3 \text{ A}$  the perpendicular magnetic field  $B_{\perp w}$  is 14.5 G on the axis of a 1.1 cm radius beam pipe. Upon exiting the wiggler region, the electron beam is adiabatically compressed into the high magnetic field region ( $B_{z0}=6.42 \text{ kG}$ ) where the CARM interaction takes place. The rf power is coupled out through a matched quartz window.

Using a wiggler trajectory code and conservation of the adiabatic moment, for the experimental conditions corresponding to the maximum rf power obtained, the calculated  $\alpha$  value ( $\alpha = \beta_{\perp}/\beta_z$ ), evaluated at the entrance of the interaction region, is  $\alpha_{th}=0.35$ , and the corresponding parallel momentum spread is  $\sigma_{pz}/p_z=5\%$ . The electron beam dynamics inside the wiggler region induces a beam-centroid displacement with respect to the waveguide axis. For the typical experimental parameters, the total displacement is approximately 3 mm, of which 1.5 mm of the displacement is due to the wiggler dynamics and 1.5 mm to possible mechanical misalignment.

To provide frequency-selective feedback to the growing waves a Bragg cavity was used. The Bragg resonator [17-19] is designed to provide feedback in the fundamen-

tal circular  $\text{TE}_{11}$  mode at frequencies considerably higher than the cutoff frequency of the waveguide used (resonant frequency,  $\omega_r/2\pi=27.8 \text{ GHz}$ , and cutoff frequency,  $\omega_c/2\pi=11 \text{ GHz}$ ). The cavity has been designed and analyzed as both an inhomogeneous problem and an eigenvalue problem using coupled mode theory [17]. In the cylindrical waveguide structure used in this experiment, the corrugated sections forming the Bragg reflectors are built using alternating copper rings of equal axial length but different radii. Since the corrugated section has an  $m=0$  structure, only modes with the same azimuthal index are coupled. The Bragg wavelength  $\lambda_B$  has been chosen in order to satisfy the Bragg resonant condition for the  $\text{TE}_{11}$  mode at 27.8 GHz. In order to avoid high  $Q$  modes near cutoff (gyrotron modes), the straight section smooth-waveguide radius is equal to the minimum radius of the corrugated sections. This type of Bragg resonator was successfully used in a free electron maser (FEM) experiment [12]. The Bragg resonator parameters are summarized in Table I. Notice the high quality factor  $Q_{tot}=10000$  of the  $\text{TM}_{01}$  mode (rejection-band mode). Cold test measurements of the resonant frequencies of the longitudinal  $\text{TE}_{11}$  modes were in very good agreement with the frequencies predicted by the cold cavity code.

In most experiments using cyclotron resonance, a critical parameter is the beam  $\alpha$ . In order to measure experimentally this parameter we make use of a capacitive probe [20] which is placed after the adiabatic compression. When the electron beam is present, the potential difference between the inner and outer capacitor plates,  $\Delta\Phi$ , is proportional to the ratio  $I_b/\langle v_z \rangle$ , where  $I_b$  is the transmitted beam current and  $\langle v_z \rangle$  is the mean parallel velocity. The calibration of the probe has been made by measuring  $\Delta\Phi$  versus beam voltage with no wiggler field ( $\alpha=0$ ). In this case, the relative variation of the measured signal,  $\Delta\Phi$ , is consistent with the theoretical value. When the wiggler field is set to the operating value, for a fixed beam voltage and beam current, the mean beam  $\alpha$  is deduced by measuring the relative change of  $\Delta\Phi$  from the case with no wiggler field.

TABLE I. CARM oscillator Bragg resonator parameters.  $N_1$  and  $N_2$  are the number of Bragg periods of the gun-side and window-side reflectors, respectively. The quantities  $\omega_r/2\pi$  and  $Q_{tot}$  are the resonant frequency and total quality factor, respectively.

Number of Bragg periods	$N_1=69, N_2=21$
Small ring radius	$r_1=7.94 \text{ mm}$
Large ring radius	$r_2=8.71 \text{ mm}$
Bragg wavelength	$\lambda_B=5.84 \text{ mm}$
Straight section length	$L=2 \text{ cm}$
Cavity cutoff $\text{TE}_{11}$	11.06 GHz
Cavity cutoff $\text{TM}_{01}$	14.46 GHz
$\omega_r/2\pi, Q_{tot}$	27.2 GHz, 390 ( $\text{TE}_{11}$ )
(Axial modes)	27.8 GHz, 300 ( $\text{TE}_{11}$ )
	28.3 GHz, 390 ( $\text{TE}_{11}$ )
	29.6 GHz, 10000 ( $\text{TM}_{01}$ )

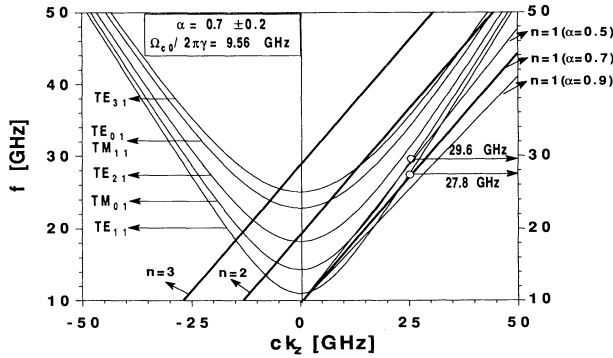


FIG. 2. Uncoupled dispersion relation for different TE and TM waveguide modes and harmonics ( $n=1,2,3$ ) of the cyclotron frequency. The pitch  $\alpha=0.7(\pm 0.2)$  and the axial guide field is  $B_{z0}=6.42$  kG corresponding to a relativistic cyclotron frequency of  $\Omega_{c0}/2\pi\gamma=9.56$  GHz. The two open dots correspond to the measured frequency for the  $TE_{11}$  and  $TM_{01}$  modes. Corresponding to the  $\alpha$  error bar, the upper and lower limits for the  $n=1$  beam line are drawn.

The microwave circuit for the frequency and power measurements is based on a tunable frequency-locked band-pass filter (20–40 GHz, filter bandwidth  $\Delta f=60$  MHz) and a careful measurement of the attenuation factors of different microwave components. For the power measurement, the tunable frequency-locked band-pass filter (insertion loss  $-13$  dB at 27.8 GHz) was placed after both a calibrated  $TE_{11}$  directional coupler ( $-60$  dB  $\pm 0.5$  dB at 27.8 GHz) and a variable attenuator (0–60 dB  $\pm 0.1$  dB) in order to ensure that only one mode was detected by a calibrated diode. The overall accuracy of this power measurement is estimated to be  $\pm 2$  dB.

The capacitive probe diagnostic shows that for the experimental setting the beam pitch  $\alpha$  is significantly larger than the value predicted by both the single particle theory and the wiggler simulation code. Within the accuracy of our measurement we measured an  $\alpha_{exp}=0.7(\pm 0.2)$  at the entrance of the interaction region, which is larger than the theoretical value of  $\alpha_{th}=0.35$ . Experimental indications suggest that the discrepancy between the measured and computed  $\alpha$  values might be due to beam instabilities in the wiggler and adiabatic compression region. As shown in Fig. 2, the experimentally determined  $\alpha$ ,  $\alpha_{exp}$ , is consistent with the uncoupled dispersion relation between the beam mode [Eq. (1)] and the waveguide mode [Eq. (2)] and the observed frequency of 27.8 GHz corresponding to the  $TE_{11}$  rejection-band mode.

The measured rf signals have shown an important competition between the designed  $TE_{11}$  mode at 27.8 GHz and a  $TM_{01}$  mode at 29.6 GHz. These two frequencies are in very good agreement with the theoretical frequencies predicted by a cold resonator code. A typical rf diode signal and voltage pulse wave form are shown in Fig. 3. The rf power shown in this figure corresponds to

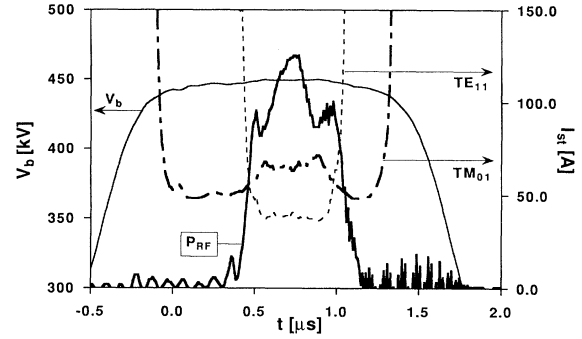


FIG. 3. Typical rf diode signal ( $P_{rf}$ ) and voltage pulse wave form ( $V_b$ ). The rf signal is proportional to the total power integrated over all frequencies above the waveguide cutoff frequency (21.08 GHz). The peak in the center of the wave form is the 27.8 GHz signal ( $TE_{11}$  mode) and its peak value corresponds to a power of 1.9 MW. Also shown are the theoretical curves for starting current versus time for the  $TE_{11}$  and  $TM_{01}$  modes.

the total power and is measured with the directional coupler; the center peak corresponds to the  $TE_{11}$  mode whereas in the left and right wings a contribution of the  $TM_{01}$  mode has been observed. A systematic excitation of the  $TM_{01}$  mode before the  $TE_{11}$  mode has been observed and can be explained by time variations of  $\alpha$  during the high-voltage pulse. The beam  $\alpha$  varies during the pulse as a result of a 0.5% variation of the modulator voltage pulse. By calculating the starting current versus time (see Fig. 3) for both modes, due to this  $\alpha$  variation and assuming a total beam-centroid displacement of 3 mm, one can show that the  $TM_{01}$  mode becomes unstable approximately 500 ns before the  $TE_{11}$  mode. This important time difference is sufficient for the  $TM_{01}$  to reach equilibrium before the  $TE_{11}$  despite the fact that the rise time of the  $TM_{01}$  ( $Q/\omega \approx 50$  ns) mode is much longer

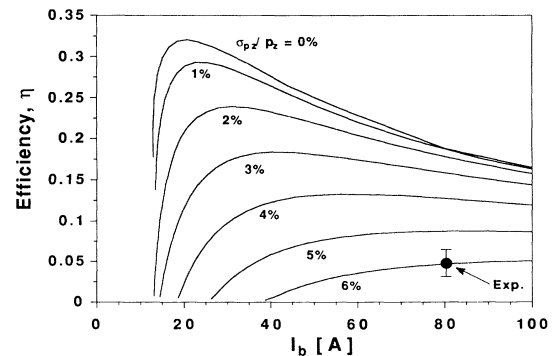


FIG. 4. Computed nonlinear efficiency versus beam current for different parallel momentum spread in the beam, based on single-mode theory ( $TE_{11}$ ). The solid circle corresponds to the measured power of 1.9 MW at  $I_b=80$  A and agrees with theory for a  $\sigma_{pz}/p_z \approx 4.5\%$ .

than the rise time of the TE<sub>11</sub> mode ( $Q/\omega \approx 1$  ns).

For the experimental conditions, the nonlinear efficiency is calculated for the TE<sub>11</sub> mode from single-mode theory [21] assuming a longitudinal rf field profile of the forward wave as being that given by the cold cavity eigenmode code. For this mode, the nonlinear efficiency versus beam current is shown in Fig. 4 for different parallel momentum spreads  $\sigma_{p_z}/p_z$ . The measured rf power for the TE<sub>11</sub> mode is 1.9 MW ( $\pm 700$  kW) and corresponds to a nonlinear efficiency of 5.2% ( $V_b = 450$  kV,  $I_b = 80$  A) which is consistent with theory for a parallel momentum spread of  $\sigma_{p_z}/p_z \geq 4.5\%$  (Fig. 4). The transmitted beam current was  $\sim 100\%$  of the cathode current.

Despite shot-to-shot power fluctuations, the maximum measured power of 1.9 MW has been found to be reproducible. A consequence of operating the CARM with phase velocities very close to unity ( $\beta_{ph} = 1.087$ ) is that small fluctuations in beam parameters strongly influence the interaction. From a scan of the far-field radiation pattern, the estimated power in the TM<sub>01</sub> is of the order of 40 kW. Since the quality factor for this mode is very large ( $Q_{tot} \approx 10000$ ) compared to the TE<sub>11</sub> mode ( $Q_{tot} \approx 300$ ), the circulating power in the cavity for the TM<sub>01</sub> mode is comparable with the circulating power of the TE<sub>11</sub> mode, which suggests that the competing TM<sub>01</sub> mode may affect the overall CARM efficiency as has been observed in gyrotrons [22].

Operation of a long-pulse high-power CARM oscillator has been demonstrated. An rf power up to 1.9 MW has been measured in the designed TE<sub>11</sub> mode at a frequency of 27.8 GHz. The corresponding efficiency is 5.2% ( $V_b = 450$  kV,  $I_b = 80$  A). Theory is in agreement with the observed output power. Simultaneous emission of a TM<sub>01</sub> mode was observed with the TE<sub>11</sub> mode. Beam quality improvements together with the suppression of the unwanted competing TM<sub>01</sub> mode, by operating at grazing condition [4,21], should allow the realization of higher efficiency CARMs ( $\sim 20\%$ ) which are relevant for electron cyclotron heating of fusion plasmas.

W. J. Mulligan and G. Yarworth provided invaluable technical assistance. This work was supported by the

Department of Energy, Advanced Energy Projects Office, under Contract No. DE-FG02-89ER14052. Additional support from Thomson Tubes Electroniques and Ferretec, Inc. is gratefully acknowledged. S.A. is supported by Swiss National Science Foundation Fellowship No. 8220-30665 and J.L.R. is supported by CEA/CESTA, France.

\*Also with Thomson Tubes Electroniques, Vélizy, France.

- [1] K. E. Kreischer and R. J. Temkin, *Phys. Rev. Lett.* **59**, 547 (1987).
- [2] W. Lawson *et al.*, *Phys. Rev. Lett.* **67**, 520 (1991).
- [3] M. I. Petelin, *Radiophys. Quantum Electron.* **17**, 686 (1974).
- [4] V. L. Bratman *et al.*, *Int. J. Electron.* **51**, 541 (1981).
- [5] A. T. Lin, *Int. J. Electron.* **57**, 1097 (1984).
- [6] J. G. Wang *et al.*, *IEEE Trans. Plasma Sci.* **17**, 906 (1989).
- [7] V. L. Bratman and G. G. Denisov, *Int. J. Electron.* **72**, 969 (1992).
- [8] K. D. Pendergast *et al.*, *Int. J. Electron.* **72**, 983 (1992).
- [9] J. Walsh *et al.*, *Phys. Rev. Lett.* **53**, 779 (1984).
- [10] T. J. Orzechowski *et al.*, *Phys. Rev. Lett.* **58**, 2172 (1986).
- [11] M. E. Conde and G. Bekefi, *Phys. Rev. Lett.* **67**, 3082 (1991).
- [12] B. G. Danly *et al.*, *Phys. Fluids B* **4**, 2307 (1992).
- [13] A. A. Kolomenski and A. N. Lebedev, *Dokl. Akad. Nauk SSSR* **145**, 1259 (1962) [*Sov. Phys. Dokl.* **7**, 492 (1962)].
- [14] A. C. DiRienzo *et al.*, *Phys. Fluids B* **3**, 1755 (1991).
- [15] I. E. Botvinnik *et al.*, *Pis'ma Zh. Tekh. Fiz.* **8**, 1386 (1982) [*Sov. Tech. Phys. Lett.* **8**, 596 (1982)].
- [16] V. L. Bratman *et al.*, *IEEE J. Quantum Electron.* **19**, 282 (1983).
- [17] G. G. Denisov and M. G. Reznikov, *Radiophys. Quantum Electron.* **25**, 407 (1982).
- [18] M. C. Wang *et al.*, *Appl. Phys. Lett.* **48**, 817 (1986).
- [19] D. B. McDermott *et al.*, *IEEE Trans. Plasma Sci.* **20**, 393 (1992).
- [20] W. C. Guss *et al.*, *J. Appl. Phys.* **69**, 3789 (1991).
- [21] A. W. Fliflet, *Int. J. Electron.* **61**, 1049 (1986).
- [22] W. C. Guss *et al.*, *Phys. Rev. Lett.* **69**, 3727 (1992).